frontiers | Frontiers in Environmental Science

TYPE Original Research
PUBLISHED 06 December 2024
DOI 10.3389/fenvs.2024.1479824

OPEN ACCESS

EDITED BY
Alessandro Michele Hering,
Federal Office of Meteorology and Climatology, Switzerland

REVIEWED BY
Eduardo Landulfo,
Instituto de Pesquisas Energéticas e Nucleares (IPEN), Brazil
Andrew Heymsfield,
National Center for Atmospheric Research (UCAR), United States

*CORRESPONDENCE
Carme Farnell Barqué,
carme.farnell@gencat.cat

RECEIVED 12 August 2024
ACCEPTED 11 October 2024
PUBLISHED 06 December 2024

CITATION
Farnell Barqué C, Rigo T, Martin-Vide J and Úbeda X (2024) Internal structure of giant hail in a catastrophic event in Catalonia (NE Iberian Peninsula).
Front. Environ. Sci. 12:1479824.
doi: 10.3389/fenvs.2024.1479824

Internal structure of giant hail in a catastrophic event in Catalonia (NE Iberian Peninsula)

Carme Farnell Barqué[1]*, Tomeu Rigo[1], Javier Martin-Vide[2] and Xavier Úbeda[2]

[1]Meteorological Service of Catalonia, Barcelona, Catalonia, Spain, [2]Department of Geography, Universitat de Barcelona, Barcelona, Catalonia, Spain

Introduction: On 30 August 2022, a giant hail-bearing supercell hit Catalonia (NE Iberian Peninsula), producing stones 12 cm in diameter. This is the most severe episode ever recorded in the country. Seventy people were injured, resulting in one fatality; several buildings were severely damaged, which resulted in substantial financial losses (more than €6M).

Methods: In the present study, we analyze the stones collected during fieldwork to gather information on their growth processes. This analysis was conducted considering two lines of investigation. In this paper we focus on the innovative and never-before-used technique of the Computed Tomography Scan, which was utilized to analyze hailstones and their interiors, the outcomes were groundbreaking. It makes it possible to obtain a complete 3D view of the interior of the stone, without producing any alteration in the structure. Through this technology, the different layer densities have been quantified. This is the main novelty of the study and opens a promising door to more analyses in this field.

Results: The analysis has revealed some interesting results that help to verify previous theories. For instance, the nuclei can be placed far from the stone center, even if the hailstone is externally spherical.

Discussion: Besides, a thicker hailstone layer in one direction indicates the falling direction. Finally, the different layer densities show growth process variations.

KEYWORDS

hailstone, fieldwork, internal structure, CTS, hail layers, hail growth

1 Introduction

On 30 August 2022, Catalonia (NE Iberian Peninsula) recorded the largest hailstones it has ever seen in at least the last 30 years (Farnell et al., 2023; Rigo and Farnell, 2023c; Rigo and Farnell, 2023b). A supercell, hereafter labeled as TH produced copious amounts of large hail, including giant hailstones (12 cm of diameter, according to some validated photographs that included a reference object), causing significant destruction, with one fatality, over 70 injuries, and extensive damage to cars and the roofs of buildings. Thanks to a campaign started by the Meteorological Service of Catalonia in 2018 (Farnell et al., 2022), many spotters and other citizen people provided us of pictures of the event. Some of these spotters also contacted us indicating that they have collected in their fridges different samples of the fallen hailstones. As it will presented later, the hailstones had diameters between 4.5 and 8.5 cm, being quite representative of the general registers at least on the

region of interest (Rigo and Farnell, 2023a). This was the starting point of our research, focused on the understanding of the growing processes inside the TH and based on the analysis of the internal structure of those stones.

The hailstone and its internal layers are the result of the various meteorological conditions encountered by the particle within the vertical axis of the TH. This takes place mainly during the growing phase, where stones collect a large set of cloud droplets and liquid drops (Fan et al., 2018).

The hailstones are composed of different layers and an embryo. The embryos are particles smaller than 1 cm in diameter and are crucial for further growth (Knight, 1981; Heymsfield, 1982; Knight and Knight, 1970a; List and de Quervain, 1953, among others). Embryo formation and subsequent growth occur during storms with robust updrafts capable of carrying microparticles to higher altitudes where temperatures are below freezing (Rauber et al., 2005). In the case of the presented event, the updraft of the TH reached 72 m/s when giant hail was recorded, according to Farnell et al. (2023).

Hailstones grow in different ways depending on the available liquid water content, ambient temperature, surface temperature, and size. The two main regimes are known as "dry growth" and "wet growth" processes (Ludlam, 1958), which describe whether the hailstone surface during growth is ice or liquid, respectively. As a rule, the wet-growth process generates clear ice, as air bubbles have had an opportunity to combine and escape. On the contrary, air bubbles become trapped during the dry-growth stages, producing cloudy-white or opaque rings of ice (Knight and Knight, 2005).

Hailstones' shape has been an object of study since the early sixties of the last century. It is a relevant issue because of its implication in many fields, such as radar reflectivity estimation (Kumjian, 2013), and the terminal fall velocity (Heymsfield and Wright, 2014), among others.

Knight (1986) determined that the sphericity (or the relationship between the three axes that characterize the volumetric shape of the stone) decreased with the size. That analysis was conducted with a set of stones with a maximum diameter of 5 cm. In the same way, Farnell et al. (2022) analyzed the external shape of a set of hailstones in Catalonia through photographs. The research divided stones in embryos-like, irregular (this is, with many lobes around the nuclei), and spherical. This study coincided with the previous one, confirming that as larger the hail, the more irregular the external shape was.

There are multiple techniques used for the analysis of the stone, most of them from an optical perspective, using simple photography (Soderholm and Kumjian, 2023) or transmitted light or cross-polarized light (Michaud et al., 2014) of thin layers (usually lower than 3 mm). Giammanco et al. (2017) used laser 3D scanning techniques which allowed determining easily the external shape of hailstones. Besides, they estimated differences in radar reflectivity between real stones and perfect spherical bodies (Jiang et al., 2019).

Other studies have focused on the analysis of the internal structure of hailstones attempting to establish the density of the different layers with the use of an instrument based on the Archimedes principle (Knight and Heymsfield, 1983). Hailstones density constitutes a crucial parameter in their structure analysis because it provides basic information on the growth process, as summarized in Allen et al. (2020). Most of the preliminary studies in the nineteen sixties and nineteen seventies in the United States mainly involved the use of polarized photography and ordinary transmitted light (Bailey and Macklin, 1968; Knight and Knight, 1970b; Macklin et al., 1976). The photography enabled the different layers inside the stones to be observed, including the air bubbles existing in some parts of the structure; this made possible the development of growth theories that discriminate between dry and wet conditions. The research conducted by Shedd et al. (2021) was the continuation of the original work; it involved the use of new and more sophisticated techniques, including 3D scanning of hailstones. More recently, Kozjek et al. (2023) studied the composition of giant hailstones, using scanning electron microscopy and Raman spectroscopy.

Going beyond the literature explained previously, we attempt to conduct an in-depth examination of the internal structure of the hailstones and quantify the different densities that would explain the processes the hailstone experienced during its formation. We achieved it by applying a technology that has never been applied before in this topic: a computed tomography scan (CTS). Then, the main objective of this research is to show the capabilities of this technique. In this way, we present the conducted methodology and, on the other hand, we show the first results of how it can be applied to determine some growing behaviors of the stones.

Our paper is divided into two parts: first, the field observations presentation to identify the location of the samples, and to explain their characteristics. Then, an analysis of the hail structure through a CTS. This has allowed to explain some of the processes occurring during hail formation. This study has also considered an objective analysis through density values.

2 Data and methodology

2.1 Area of study

Catalonia is situated in the northeast of the Iberian Peninsula (Figure 1). The region is characterized by the Pyrenees and Pre-Pyrenees mountain ranges, which run roughly parallel to each other in an east-west direction. These mountain ranges reach altitudes of over 3,000 and 2,500 m, respectively. Their steep slopes create favorable conditions for the initiation and development of convection in unstable environments (Rigo et al., 2022). Additionally, Catalonia's coastline extends from the southwest to the northeast, with the Mediterranean Sea exerting a significant influence on the region's climate; this results in relatively mild atmospheric temperatures and, in certain cases, gives rise to abundant moisture.

The Empordà region is situated in the northeast of Catalonia (included in the black rectangle in the left-right panel of Figure 1). This is where the Pyrenees and the Pre-Pyrenees reach the Mediterranean Sea. Here the ranges do not exceed 1,400 m and some areas along the coast present minimum altitudes and a flat terrain.

2.2 Hail records

The reports employed in the present study were provided in Rigo and Farnell (2023b). The database includes records of severe

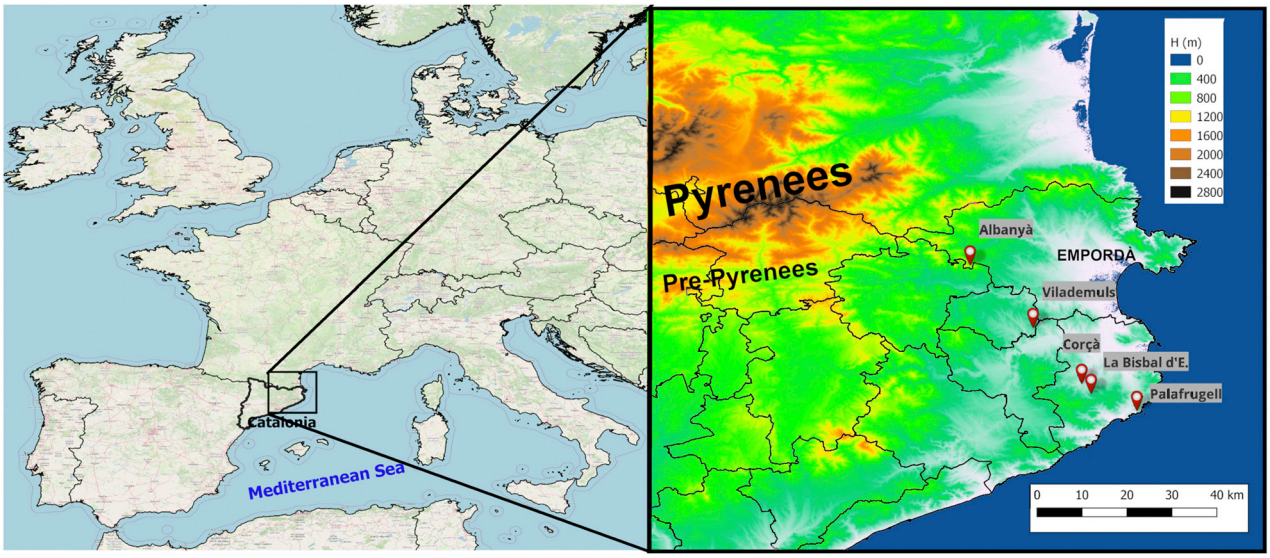

FIGURE 1
Study area. Catalonia is located (black square) on the map on the left-hand side in relation to the rest of Europe. The map on the right shows the area affected by the hailstorm, along with the municipalities possessing records of the size of the hailstones (blue triangles). The red circles are the municipalities in which we collected the stones to conduct the subsequent analyses. The background color represents the elevation above sea level in the study area.

weather phenomena such as tornadoes, downbursts, large hail, and straight-line convective winds, dating back to 2004. It also contains information on small hail. This wealth of information enabled the creation of a severe weather climatology for Catalonia, which permitted us to determine the exceptional nature of the hailstorm under analysis.

The largest hailstones occurred in 2009, 2012, and 2014, with a maximum diameter of 7 cm. In 2007, 2020 (twice), and 2022 (three times before the event under investigation), the maximum diameter was close to 6 cm. However, the event under study contained the largest hailstones ever reported in the area, measuring 12 cm. Furthermore, database records also show an increase with time in the size of hailstones reported in Catalonia.

Regarding the TH, some observers collected the hailstones and kept them in their freezers. By means of a survey conducted on social media, 14 hailstones were collected and subjected to different analyses, such as chemical and imagery. Moreover, numerous citizens took photos and videos during the TH in different parts of the affected area, sharing them on social media or through the Meteocatpedra campaign (Farnell and Rigo, 2020).

The hailstorm developed in a scenario marked by the pass of a small trough at 300 hPa between 12.00 and 18:00 UTC. There was also a slight intrusion of the troposphere and a light reinforcement of the jet stream over the region of interest. Besides, the mesoscale was marked by the wind convergence at low levels in the convection initiation region. This convergence was caused by the interaction between sea (South-Eastern) and land (Western) wind flows at low levels. More information about the mesoscale and synoptic scenarios where the supercell grew, develop and moved can be found in Farnell et al., 2023.

The axes of most hailstones were measured during packaging and before transport to the central offices. We measured the vertical, horizontal, and thickness axes (3D dimensions) and the weight (mainly for the third sample set). The axes measurements allowed the identification of the stone shape used to infer their sphericity. This measurement consists of the sphericity index estimation. In this way, if the lengths of the three representative axes of a hailstone are: the longest (a), the intermediate or mid axis (b), and the shortest (c), a widely accepted sphericity index is the following (Sneed and Folk, 1958; Cruz-Matías et al., 2019):

$$\Psi = (c^2/ab)^{1/3}$$

A sphericity value close to one indicates that the hailstone has an approximate spherical shape.

Unfortunately, it was impossible to make all the measurements for the first two sets due to logistical issues in the stones' packaging and transport processes. On the contrary, all fourteen samples from the observer Joan have 3D measurements (see more in Table 1).

2.3 Computed tomography scan (CTS)

One phase of the research consisted of internally analyzing a set of available hailstones. We decided to test a novel technique involving the use of medical imagery, rather than the proposed state-of-the-art methodologies. The samples were obtained by means of computed tomographic cone beam scanning (TCS) of the three-dimensional structure, in a similar way to dental photographs. The files have the DICOM (Digital Imaging and Communications in Medicine) format (more information can be found, for instance in Whitcher et al., 2011).

The recently conducted scan has been carried out with a set of specific parameters to ensure precise image acquisition. With a wide

TABLE 1 Size measured with a caliper thorough major axis, "a," middle axis, "b," and minor axis, "c," weight, and sphericity of the hailstones collected during the fieldwork. The error in the axis length is the 3% of its value, according to international standards about spheroid measurements. Italic text cells correspond to hailstones studied through the internal scattering of their structure.

	Major axis -a- (cm)	Mid axis -b- (cm)	Minor axis -c- (cm)	Weight (g)	Sphericity
La Bisbal d'Empordà					
(Observer: Manel)					
Sample 1	7.5	6.0	NA	66.0	NA
Sample 2	4.5	4.2	NA	NA	NA
Sample 3	6.3	5.0	NA	NA	NA
Sample 4	6.2	5.3	NA	NA	NA
(Observer: Jesús)					
Sample 1	7.0	4.5	NA	86.0	NA
Sample 2	5.0	4.0	NA	NA	NA
Corçà					
(Observer: Joan)					
Sample 1	8.5	7.0	5.0	143.0	0.8
Sample 2	8.5	8.0	2.5	NA	0.5
Sample 3	6.3	6.0	4.0	NA	0.8
Sample 4	7.0	6.4	4.7	NA	0.8
Sample 5	8.3	6.9	4.0	126.0	0.7
Sample 6	5.7	5.5	3.5	102.0	0.7
Sample 7	7.0	5.0	4.5	27.0	0.8
Sample 8	6.5	5.4	3.5	NA	0.7
Sample 9	6.0	5.0	2.0	64.0	0.5
Sample 10	6.1	5.4	4.9	NA	0.9
Sample 11	6.0	5.2	3,6	89.0	0.8
Sample 12	6.0	4.5	1.5	30.0	0.4
Sample 13	5.0	4.2	1.8	25.0	0.5
Sample 14	4.6	4.5	1.5	28.0	0.5

range of configurations, the result is a detailed and sharp representation of internal hailstone structures.

This type of analysis allowed us to obtain 3D imagery of the external structure. Furthermore, it enabled the acquisition of internal information; each volume is divided into 512 horizontal slices. All this information collectively creates the 3D volume (see Figure 2). The slice width of each slice is 0.16 mm, which allows exceptionally high resolution in the obtained images. The peak kilovoltage (KVP) was set to 85 to ensure adequate penetration of X-rays through body tissues. This optimal energy level allows for excellent differentiation of densities. The detailed images were ensured by an exposure time of 3,200 milliseconds. This extended exposure duration is crucial for obtaining high-quality images, especially in areas of interest that require greater clarity and resolution. Finally, setting the X-ray tube current to 7 mA ensured consistent emission of X-rays during the scan. The software used in this study was Onis 2.6.

The study focused on the high-resolution analysis of the Hounsfield Units (hereafter, HU) in different parts of the stones (Peralta et al., 2019), which helped us to determine diverse elements of the structure: location of the embryos, distribution of the different layers (and their density), and whether or not air bubbles are trapped inside.

The Hounsfield Units (HU) are a measure of X-ray attenuation used mainly in computed tomography scan (CTS) or X-ray scanners. These units are defined in relation to the attenuation of water and air. Water is defined as having an attenuation of 0 HU, while air is defined as −1000 HU.

An inconvenience that we have to consider about this technology is the Beam hardening, known as Blooming artifact (Pack et al., 2022). This artifact occurs when an extremely dense object, absorbs a significant X-rays amount, causing radiation detectors to saturate and produce overexposure in surrounding

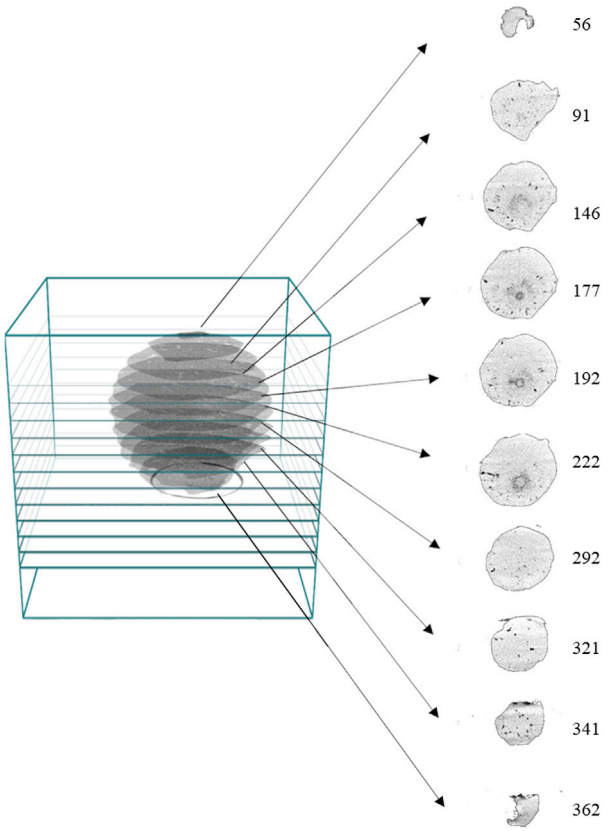

FIGURE 2
An illustration exemplifying the CTS analysis method is depicted. On the left, a 3D volume is shown, while on the right, various slides dividing the volume are displayed.

areas. In the presented analysis we did not detect this artifact occurrence in the imagery of the stone. Besides, the high contrast between the regions with hail and the outer areas made the identification of the stones' borders easier. Then, in opposition to Shedd et al. (2021) technique using Laser Infrared scans that presented errors in the size estimation, the measurement precision allowed us to have the same values of the axes compared with the direct estimations.

2.4 Field observations

On 30 August 2022, the TH originated in the French Pyrenees. The storm moved from the NW to the SE, crossing part of the Catalan Pyrenees until it reached the Mediterranean Sea. During this trajectory, large hailstones were observed and recorded in five villages (see right panel Figure 1); they presented a maximum diameter of 12 cm.

The fieldwork first entailed getting in touch with the observers who had kept the hailstones in their freezers. Subsequently, different tools were employed to gather these hailstones in the best possible manner. The instruments were a foot ruler, vacuum packaging, labels, and expanded polystyrene boxes filled with salt.

The following steps were taken: 1. We measured the diameter and weight of the stones. 2. We took notes and labeled the samples. 3. The stones were placed in a plastic bag, which was vacuum sealed. 4. The stones were kept in an expanded polystyrene box. Figure 3 illustrates some steps of the process.

The axes, weight, and thickness were calculated for the 14 hailstones collected (see Table 1). Moreover, the axes are shown with yellow lines, in the right part on Figure 5). The measurement of the different axes in the three dimensions allowed us to determine the sphericity of the stones, which is shown in the last column of Table 1. We could divide the set of 14 samples into two categories, depending on the exceeding of the threshold: spherical ($\Psi > 0.7$, following the recommendations of Cruz-Matías et al., 2019) and non-spherical hailstones. Nine of the stones were spherical (64 %), while the rest had a non-spherical shape. The different parameters (maximum, minimum length axis, or weight) had different correlation values with the sphericity of the stones: 0.277, 0.949, and 0.611, respectively. These values indicate that the best correlated parameter was the minor axis longitude, implying that as larger this dimension, the more spherical the hailstone. In general, hailstones with a minor axis exceeding 3.5 cm have a sphericity index over 0.7 (only one exception did not satisfy this condition). These values are in the same line that the obtained Shedd et al. (2021), which studied a higher number of samples but with sphericity values ranging between 0.57 and 0.99. Finally, it is worth noting that the maximum recorded weight was 143 g.

2.5 Hail analysis structure by computed tomography scan

The CTS analysis was conducted on three samples collected during fieldwork (see Figure 4). The pieces were selected randomly, and their characteristics can be seen in Table 1, highlighted in italic text. Each of the pieces was analyzed considering all 3D information, comprising 512 slides, to locate the nuclei and the different layers according to their density. In this context, and in accordance with the literature explained previously in the introduction, the layers were defined considering the strong color contrast between areas and elongated air bubbles. For each area, a density histogram was created to corroborate the differences between them.

It is crucial to take into account that the opaque layer in the stone contains more air and has less density. In the CTS process, this layer appears dark (black) because it allows more X-rays to pass through. This results in a greater number of X-rays reaching the detector, and therefore, it appears darker in the image. On the contrary, the clear layer in the stone has more density because it contains a higher quantity of water and scant air. In the case of the CTS, this layer appears in white or gray color.

2.6 Analysis of spherical-shaped stones

At first glance, the most surprising observation of the internal structure was the heterogeneity of the stones (see Figure 5), which could not be perceived from the outside, especially in spherical stones. In this sense, the nucleus was located slightly off to one side in some of the perspectives. This characteristic is seen very evident in sample 5 (B). Furthermore, the shape was not uniform on all the axes

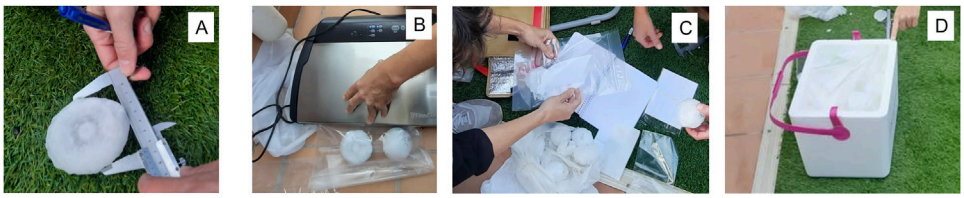

FIGURE 3
Field work involving the collection of the hailstones. **(A)** It shows how the stones were measured. **(B)** The process involves labeling each hailstone for identification purposes. **(C)** The stones were vacuum-packed to maintain the best possible characteristics thereof. **(D)** The box used to transport the hailstone during the journey from Bisbal d'Empordà to the laboratory.

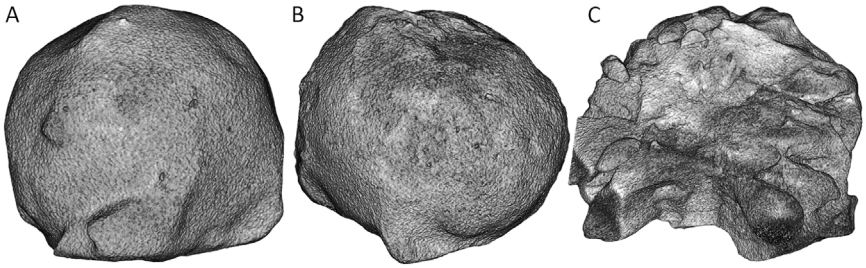

FIGURE 4
3D representation of the three samples analyzed by CTS. Left **(A)**: sample 10; Center **(B)**: sample 5; Right **(C)**: sample 2 (from Corçà by Joan). The characteristics of the samples can be seen in Table 1.

and planes, although the three-dimensional structure in sample 10 resembles a quasi-perfect sphere from the external point of view. These two points (heterogeneity and lack of sphericity in some internal layers) are the more relevant observations made in this first study. However, there are other interesting considerations to cite, listed in the following paragraphs.

Each stone has been examined departing from the nucleus location. This position has been estimated from the density field, searching for a region with high-density values. From this point, we have analyzed the internal structure considering the distance between the outermost part of the stone and the nucleus location. We have observed that samples 10 and 5 have a thicker part (see the green area and red arrows in samples 10 and 5, Figure 5). This wider area indicates the side of the stone facing downwards during the fall. In this region is where the riming accumulation favores (Knight and Knight, 1970a). On the opposite, more bubbles are detected in the thinner part. This means that this area is colder than the thicker part.

The density histograms were obtained using the ONIS software (see sample 10 shown at the top panel of the Figure 5, and the histograms in Figure 6). These histograms help to corroborate some statements. First, there are significant differences between the densities of the first, second, and third layers, particularly in the minimum values (125, 0, and −72 HU, respectively). In contrast, the density differences among the fourth, fifth, and sixth layers were not as remarkable. However, the air bubbles' structure and the hailstone's shape help to ascertain that they constituted distinct layers.

The TCS technique has the advantage of detecting with high resolution the internal air bubbles. Next, some observations regarding the bubbles are presented. For instance, the air bubble located in the fifth layer labelled B1 (highlighted in yellow), had an area of 0.018 cm^2 and its length was 4.25 mm. This bubble was more elongated than the B2 air bubble, located in the sixth layer, with a length of 3 mm, was the most significant bubble in this layer. It is worth noting that the number of bubbles in all layers was more significant in the thinner part of the stone.

Moving to the particular case of sample 5, shown in the middle panel of Figure 6, the differences between layers were more significant than for sample 10. The minimum values of densities were considerably different between the first, second, third, and fourth layers (81, −7, −61, and 14 HU, respectively). On the contrary, the fifth and sixth layers showed similar densities. However, the air bubbles in the fifth layer were more pronounced than in the sixth. In this layer, the bubbles were fewer and smaller. In any case, the boundary between both layers was well-marked. In this case, we could not detect air bubbles in the thicker part of the layer, opposite to the sample 10 observations. The last particles that adhered to the lower part of the hailstone did so through wet growth. The droplets were larger or more abundant during this part of the growth, coinciding with the conical shape of the stone (Knight, 1986).

The previous two samples, with a spherical external shape and conical internal pattern, exhibited more internal layers compared with sample 2. This observation could be related to the falling time: samples 5 and 10 fell some minutes before sample 2. This is enough for travelling inside different thermal layers during their fall because during this stage the TH showed significant changes in its structure, as was reported in Farnell et al. (2023).

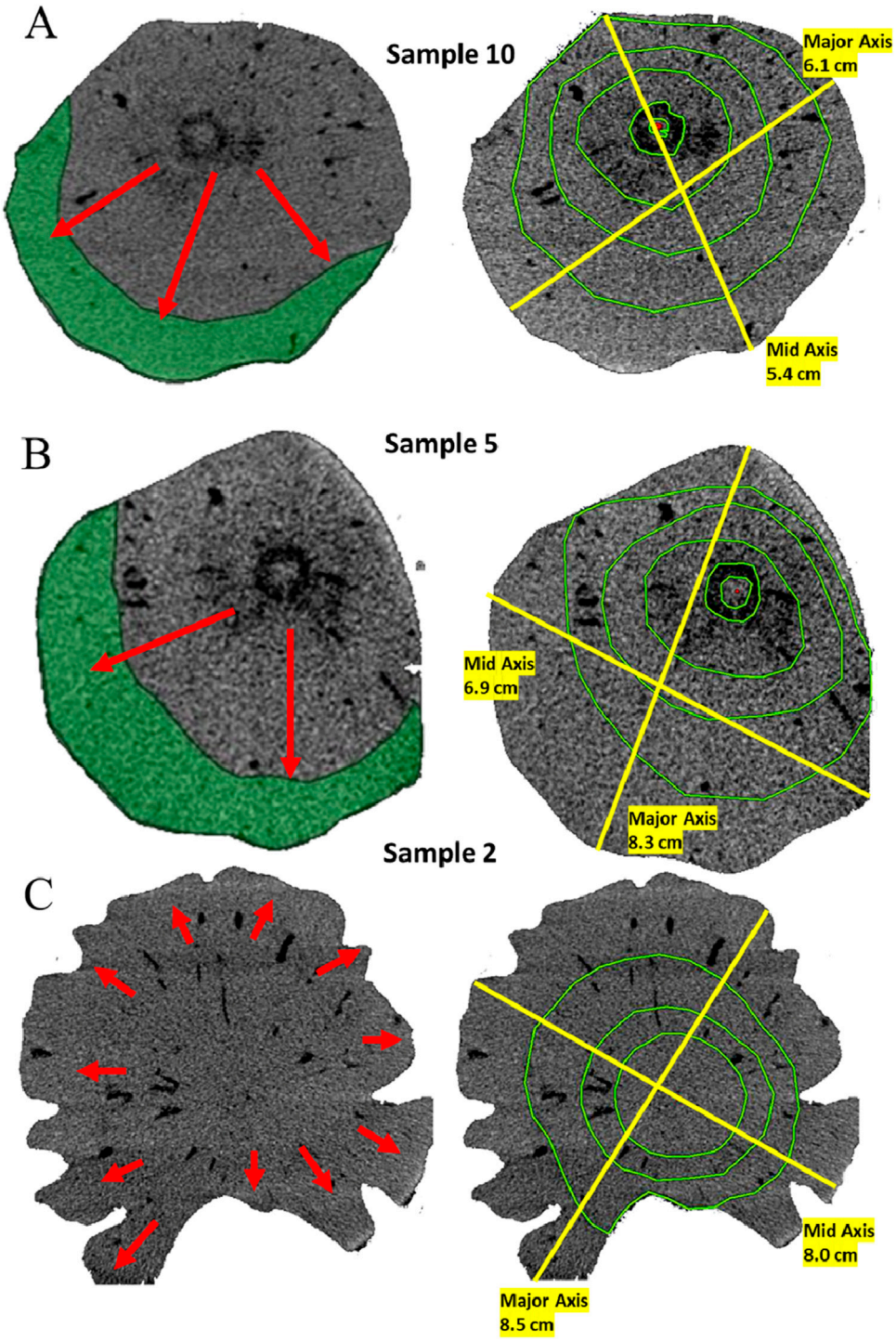

FIGURE 5
The three hail samples are seen from their interior. **(A)** sample 10; **(B)** sample 5; **(C)** sample 2.

2.7 Analysis of irregular-shaped stones

Going deeper with sample 2, it presented oblate spheroids (Figure 5) and prolates with icicle lobes (see red arrows in images C, Figure 5). According to Allen et al. (2020), the prolate form is associated with having a relatively constant falling orientation (red arrows). Because of this, it is impossible to define a meaningful average upper or lower side. The reason is that the fall and updraft speeds are counteracted; thus, the particle remains suspended at a roughly constant altitude within the hail growth region, only impacted by the lateral movement of the horizontal components of the velocity field within the updraft. That would explain why the internal layers number was lower than for samples 10 and 5. In those cases, the stones with

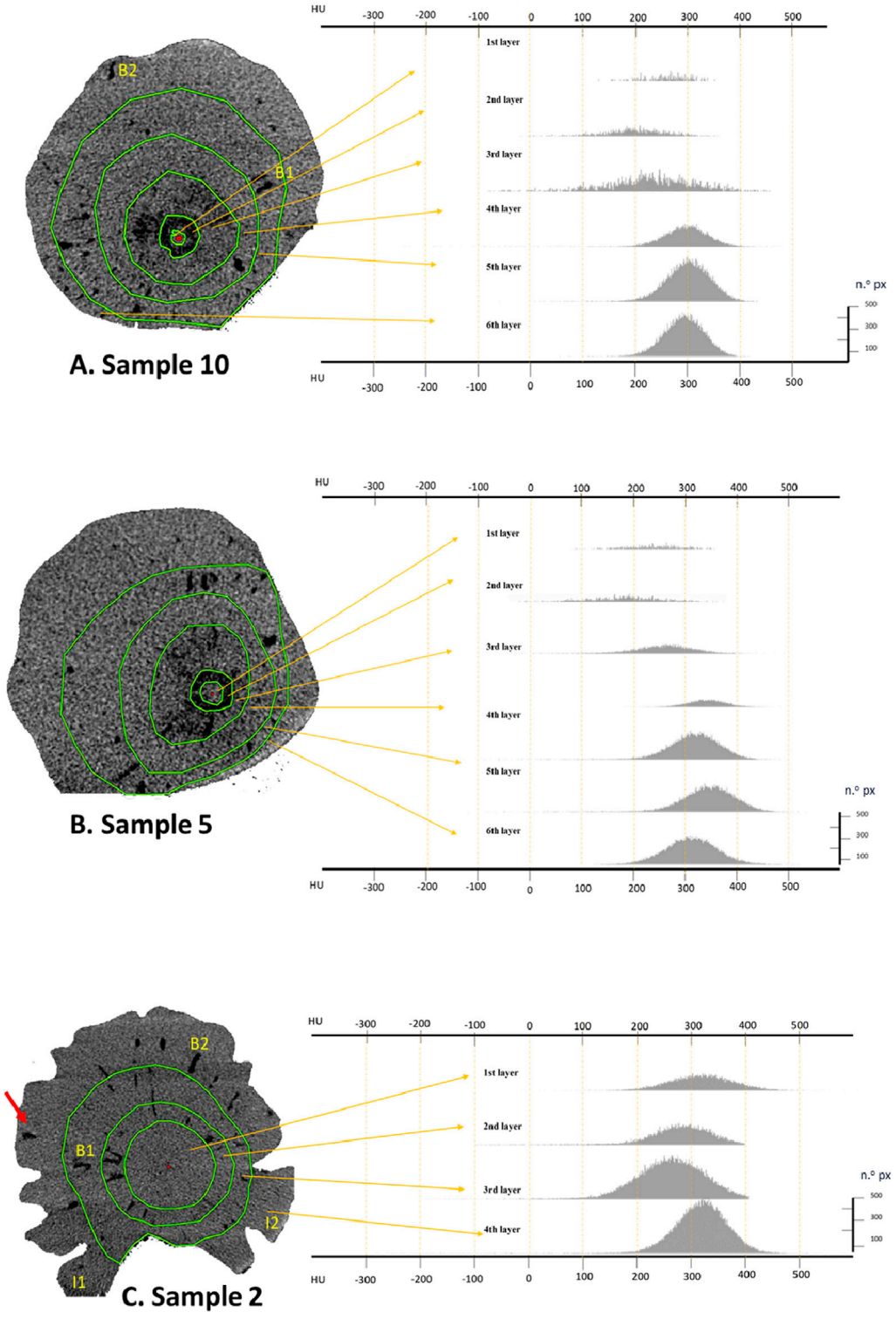

FIGURE 6
On the left, the stones are shown with their internal structure. On the right side, the density of each layer is represented through histograms. **(A)** sample 10; **(B)** sample 5; **(C)** sample 2.

spherical or oblate shapes fell crossing different thermal layers. These variations of layers are associated with dry or wet growth, generating a more complex internal structure, as stated Knight and Knight (1970b).

Furthermore, the icicle lobes observed in the external part of sample 2 exhibit a linear and radial distribution from the nucleus, similar to air bubbles. Most air bubbles appeared in the inner part of the stone, while there were scarce in the icicles. Therefore, this

hailstone grew with cold periods. However, the icicle formation occurred in a warmer phase. According to Knight and Knight (1970a) and Allen et al. (2020), icicles originate from the liquid flowing across the hailstone's surface towards the tips of the protrusions. Then, these structures appeared during the hailstone falling, created by the influence of hydrodynamic effects caused by the air stream.

The bottom panel of Figure 6 shows the few layers of stone 2, comparing with the two previous samples. If we go inside the last stone structure, the first layer is larger than the first one in previous samples; 4.67 cm^2 versus 0.06 cm^2 and 0.14 cm^2, respectively. The other layers show a clear border between them, marked by the air bubbles. For this reason, the minimum density values were negative in all of them. However, the air bubbles number in the second and fourth layers was more significant. Furthermore, they were more elongated. For example, the air bubble named B2 (highlighted in yellow), located in the fourth layer, measured 0.041 cm^2, with a length of 5.22 mm. In contrast, the B1 area (highlighted also in yellow) was 0.013 cm^2, with a length of 3.74 mm.

Finally, regarding the icicle lobes we detected high-density values in those regions. In the case of I1 (highlighted in yellow), the mean density value was 300 HU, while I2 showed a mean value of 382 HU. Although, it is possible to find some air bubbles in some protuberances (see red arrow in the same figure). However, these bubbles coincide with an area where the icicle input is missing. It could mean that this area was accumulating particles for a while longer.

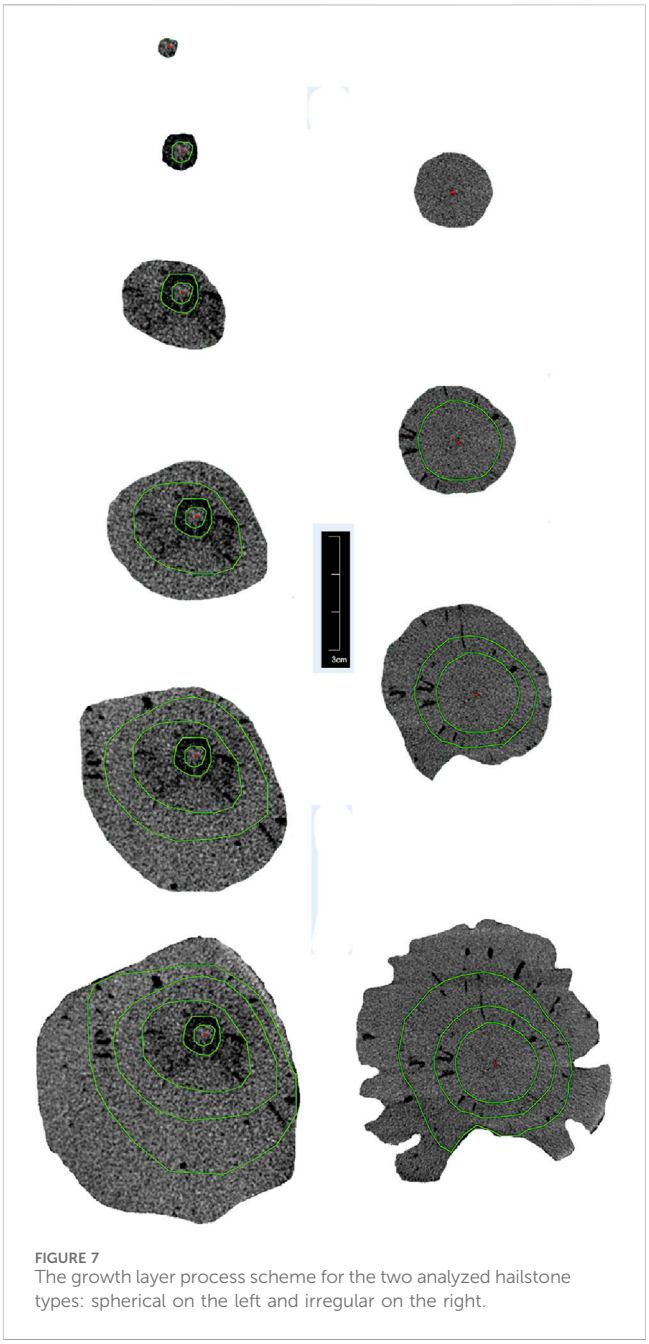

FIGURE 7
The growth layer process scheme for the two analyzed hailstone types: spherical on the left and irregular on the right.

3 Discussion

The present manuscript describes a novel technology to analyze the internal structure of the hailstones based on the application of the CTS process directly over each sample, obtaining 3D information with high resolution of the hail density, which is easy to manage with many software (from medical specialist -such as the used here- to other more general). In this section, we compare this new method with others found in the literature related to the same purpose.

The most used technique consists of taking photography of one thin layer (of less than 3 mm), in general of the central part of the stone (Michaud et al., 2014, Bailey and Macklin 1968, Knight and Knight 1970b, Macklin et al., 1976, Shedd et al., 2021; Soderholm and Kumjian 2023) went a step further and used simple software to analyze the pictures and get more information than the previous works, which only measured some characteristics using a ruler directly over the photography or, on the other hand, determined the number of bubbles per layer. The way to get the thin layer is by cutting the hailstone with a hot knife and cleaning the resulting surface. The first advantage of our technique is that we can analyze multiple layers with a similar resolution that other researchers get by direct photography, but for the whole stone. This characteristic is another advantage, as the internal distribution of the stone may differ from its external appearance. This article has presented an example where the embryo was displaced from the stone center. Then, it is necessary to do the cut properly to avoid the stone being unuseful. Anyway, the stone will no longer available after its cut. Compared with this previous technique, the proposed new method allows using a sample as many times as necessary because the internal composition does not change after the CTS application. We tested the technique twice with one stone with the result that the shape did not suffer any alteration. The unique consideration is that the stone should be threat in a cold environment to avoid external melting. Perhaps the unique negative point of using CTS instead of photography is that it is an indirect measurement, such as the get from a radar of the interior of a thunderstorm.

The laser 3D scanning techniques (Giammanco et al., 2017) allows to easily determine the external shape of hailstones with very high resolution and without damaging the sample. This method provides little better results from the exterior. However, it does not inform about the objective of our research: to know how the hailstone grew internally. Then, although the method can be

complementary to the proposed here, it cannot provides results directly.

Some old studies focused on the internal structure analysis of hailstones to determine the density of the different layers. They used an instrument based on the Archimedes principle (Knight and Heymsfield, 1983). Density is a crucial parameter to understand the growth process. The Knight and Heymsfield technique did not alter the hail composition also. Besides, it provides a direct measurement of the hail density. However, the value is unique for the entire stone and does not allow estimating the density for the different layers, as the CTS technique allows. Again, the issue of the novel method is that the density is remotely estimated.

More recently, Kozjek et al. (2023) used scanning electron microscopy with promising results. The main goal in that case was to identify the chemical composition of the hailstones. Although the spatial resolution is better than CTS, the method does not conclude anything about the growing processes. However, it can be interesting to combine both methods to get more information regarding the starting point of hail growth and even about the atmospheric composition where the stones developed.

Finally, Figure 7 shows the schematic growth layer process for the two types of analyzed hailstones (spherical and irregular). The scheme has considered the previous results and the different analyzed imagery. The main differences are the number of phases (six for the spherical and four for the irregular stone), the growing velocity (the irregular stone grows fast, according to this scheme), and how they evolve in the last stages.

4 Remarks and conclusions

On 30 August 2022, large hail (12 cm) was recorded in the northeast of Catalonia; this was the most severe episode ever recorded. Due to the importance of this episode, fieldwork was initiated to account for the evolution, trajectory, and shape of the storm and the hailstone (see Farnell et al., 2023).

Some aspects had to be considered before fieldwork. Initially, the population needed to be informed that, in the event of a hailstorm, they should collect the stones for scientists to analyze them. The most effective solution is placing them in a plastic bag and storing them in the freezer. Every year, the Catalan Government runs a campaign from May to October to inform the population (Farnell and Rigo, 2020).

The second step involved collecting the hailstones from the observers and identifying the location where they were found. Additionally, it was crucial to talk with the local population to understand the storm's path and the hailfall. Different measuring devices were employed to determine the length of the axes and to measure the weight of the stones. In addition, a freezer and a vacuum sealer were also necessary to transport the hailstones and attempt to preserve their original condition.

Two types of hailstones were identified: spherical and irregular. As observed in the axes, a 64 % of the collected hailstones were spherical, with a unique sample flat that corresponded to an irregular stone. The maximum weight recorded was 143 g. This same hailstone had a maximum axis length of 8.5 cm and a minor axis length of 7 cm, with a thickness of 5 cm. In contrast, the prolate hailstones were lighter than the spherical ones because they were significantly thinner. For example, one hailstone presented a diameter of approximately 5 cm and a thickness of 1.5 cm, with a significantly lower weight of 28 g.

The sphericity index indicates that the spherical shape appears mainly for stones with a diameter of 5 cm or less. Regarding the sphericity of the hailstones, previous studies (Knight, 1986; Giammanco et al., 2017 or Farnell et al., 2022) had observed a decrease in this parameter as the diameter increases. However, it is worth noting that these analyses only considered stones with a maximum diameter of 5 cm. In the present case, for the stones ranging from 4.6 to 8.5 cm, we have noticed that the sphericity parameter of stones with a minimum axis larger than 3.5 cm exceeds 0.7, which is the threshold imposed by Cruz-Matías et al. (2019) to consider an object as spherical-like.

An innovative technique was applied to analyze the interior of the stones and to obtain a 3D perspective of the stones. This was the Computed Tomography Scan (CTS), which can provide information that is not visible to the naked eye. It enables the acquisition of internal information and shows different density values according to the components of the stone. The densities are quantified with HU. Therefore, this technique allows us to conduct an objective analysis of the interior of hail.

It is important to remark that the opaque layer in the stone contains more air and has less density. In the CTS process, this layer appears dark (black). On the contrary, the clear layer has more density because it contains a higher quantity of water and scant air. In this case, in the CTS, this layer appears in white or gray color.

The internal structure of the stone is heterogeneous. Sample 10 and sample 5, with sphericity indices of 0.9 and 0.7 respectively, had conical interiors, more clear in sample 5.

In both cases, there was a thicker part that led to the fall. This would be the last growth phase of the hailstone. As the hailstone fell, the droplets were accreted to the lower part, did so through wet growth. We can consider this statement true because there are no air bubbles or negative HU values. On the contrary, the air bubbles are found in opposite zones, which are associated with dry growth.

Regarding the density analysis, thanks to HU values, we could differentiate the first three layers, depending on dry or wet growth (Knight and Knight, 1970b; Knight and Knight, 1970a; Allen et al., 2020). The last layers were divided considering the absence or presence of air bubbles.

Sample 2, with a prolate shape and sphericity index of 0.5, showed notable differences compared to samples 10 and 5. The prolate form is associated with having a relatively constant falling orientation due to the hailstones growth while rotating on the horizontal axis. The icicle lobes observed in the external part of the stone exhibited a linear radial distribution from the nuclei. These originated from the liquid flowing across the hailstone's surface towards the tips of the protrusions (Allen et al., 2020) with high-density values. The number of layers in its interior was lower than samples 10 and 5 due to the falling process. In sample 2, there was a moment when the stone could not fall anymore because the speed and updraft speed were matched, and the stone grew on the horizontal axis. On the contrary, the spherical or oblate stones crossed different thermal layers associated with dry growth or wet growth, generating a more complex internal structure.

Considering that the purpose is to present the novel technique of applying TCS to hailstones, the number of samples used in the current

analysis does not directly impact the results. The unique issue is the misobservation of some characteristics in the current research. In this way, future studies should be done in other places around the World to improve the knowledge regarding hail growth. Furthermore, we plan as future work the extraction of some air bubbles well-identified with the technique to know their composition and understand better the atmosphere where they formed.

Data availability statement

The raw data supporting the conclusions of this article will be made available by the authors, upon request to interested researchers.

Author contributions

CF: Conceptualization, Data curation, Formal Analysis, Investigation, Methodology, Software, Validation, Visualization, Writing–original draft, Writing–review and editing. TR: Formal Analysis, Investigation, Methodology, Supervision, Validation, Writing–review and editing. JM-V: Funding acquisition, Project administration, Supervision, Writing–review and editing. XÚ: Funding acquisition, Data curation, Investigation, Resources, Writing–review and editing.

Funding

The author(s) declare that financial support was received for the research, authorship, and/or publication of this article. This work was supported by Institut de Recerca de l'Aigua (IdRA) and Agència de Gestió d'Ajuts Universitaris i de Recerca (AGAUR) Grant: 2021SGR00859.

Acknowledgments

We wish to thank the spotters Angel Galan, Manel and Joan. Moreover, Carme Tribó, Francesc Bibiloni, and their orthodontic clinic Bibiloni-Tribó for their help and provision of material and knowledge regarding the Computed Tomography Scan images, as well as Gerard Torroella Martinez and his dental clinic. We also appreciate Silvia Rodero Lopez, cardiologist at Hospital Clinic de Barcelona and Fundació Sanitaria Mollet, for helping us to interpret the images, and Jordi Boladeras for the image processing. In addition, we would also like to express our gratitude to the Agència de Gestió d'Ajuts Universitaris i de Recerca (AGAUR) and Institut de Recerca de l'Aigua (IdRA) for financial support to publish the manuscript. We are also grateful to the Forecast and Surveillance team and the Research Area of the Meteorological Service of Catalonia.

Conflict of interest

Authors CF and TR were employed by Meteorological Service of Catalonia.

The remaining authors declare that the research was conducted in the absence of any commercial or financial relationships that could be construed as a potential conflict of interest.

Publisher's note

References

Allen, J. T., Giammanco, I. M., Kumjian, M. R., Jurgen Punge, H., Zhang, Q., Groenemeijer, P., et al. (2020). Understanding hail in the earth system. *Rev. Geophys.* 58, e2019RG000665. doi:10.1029/2019rg000665

Bailey, I., and Macklin, W. (1968). The surface configuration and internal structure of artificial hailstones. *Q. J. R. Meteorological Soc.* 94, 1–11. doi:10.1002/qj.49709439902

Cruz-Matías, I., Ayala, D., Hiller, D., Gutsch, S., Zacharias, M., Estradé, S., et al. (2019). Sphericity and roundness computation for particles using the extreme vertices model. *J. Comput. Sci.* 30, 28–40. doi:10.1016/j.jocs.2018.11.005

Fan, J., Rosenfeld, D., Zhang, Y., Giangrande, S. E., Li, Z., Machado, L. A., et al. (2018). Substantial convection and precipitation enhancements by ultrafine aerosol particles. *Science* 359, 411–418. doi:10.1126/science.aan8461

Farnell, C., Batalla, E., Rigo, T., Pineda, N., Sole, X., Mercader, J., et al. (2023). Reanalysis of giant hail event in Catalonia (NE of the iberian Peninsula). *Atmos. Res.* 296, 107051. doi:10.1016/j.atmosres.2023.107051

Farnell, C., and Rigo, T. (2020). The Lightning Jump, the 2018 "Picking up hailstones" campaign and a climatological analysis for Catalonia for the 2006–2018 period. *Tethys* 17, 10–20. doi:10.3369/tethys.2020.17.02

Farnell, C., Rigo, T., and Heymsfield, A. (2022). Shape of hail and its thermodynamic characteristics related to records in Catalonia. *Atmos. Res.* 271, 106098. doi:10.1016/j.atmosres.2022.106098

Giammanco, I. M., Maiden, B. R., Estes, H. E., and Brown-Giammanco, T. M. (2017). Using 3d laser scanning technology to create digital models of hailstones. *Bull. Am. Meteorological Soc.* 98, 1341–1347. doi:10.1175/bams-d-15-00314.1

Heymsfield, A., and Wright, R. (2014). Graupel and hail terminal velocities: does a "supercritical" Reynolds number apply? *J. Atmos. Sci.* 71, 3392–3403. doi:10.1175/jas-d-14-0034.1

Heymsfield, A. J. (1982). A comparative study of the rates of development of potential graupel and hail embryos in High Plains storms. *J. Atmos. Sci.* 39, 2867–2897. doi:10.1175/1520-0469(1982)039<2867:acsotr>2.0.co;2

Jiang, Z., Kumjian, M. R., Schrom, R. S., Giammanco, I., Brown-Giammanco, T., Estes, H., et al. (2019). Comparisons of electromagnetic scattering properties of real hailstones and spheroids. *J. Appl. Meteorology Climatol.* 58, 93–112. doi:10.1175/jamc-d-17-0344.1

Knight, C. A., and Knight, N. C. (1970a). The falling behavior of hailstones. *J. Atmos. Sci.* 27, 672–681. doi:10.1175/1520-0469(1970)027<0672:tfboh>2.0.co;2

Knight, C. A., and Knight, N. C. (1970b). Hailstone embryos. *J. Atmos. Sci.* 27, 659–666. doi:10.1175/1520-0469(1970)027<0659:he>2.0.co;2

Knight, C. A., and Knight, N. C. (2005). Very large hailstones from Aurora, Nebraska. *Bull. Am. Meteorological Soc.* 86, 1773–1782. doi:10.1175/bams-86-12-1773

Knight, N. C. (1981). The climatology of hailstone embryos. *J. Appl. Meteorology Climatol.* 20, 750–755. doi:10.1175/1520-0450(1981)020<0750:tcohe>2.0.co;2

Knight, N. C. (1986). Hailstone shape factor and its relation to radar interpretation of hail. *J. Appl. Meteorology Climatol.* 25, 1956–1958. doi:10.1175/1520-0450(1986)025<1956:hsfair>2.0.co;2

Knight, N. C., and Heymsfield, A. J. (1983). Measurement and interpretation of hailstone density and terminal velocity. *J. Atmos. Sci.* 40, 1510–1516. doi:10.1175/1520-0469

Kozjek, M., Vengust, D., Radošević, T., Žitko, G., Koren, S., Toplak, N., et al. (2023). Dissecting giant hailstones: a glimpse into the troposphere with its diverse bacterial communities and fibrous microplastics. *Sci. Total Environ.* 856, 158786. doi:10.1016/j.scitotenv.2022.158786

Kumjian, M. R. (2013). Principles and applications of dual-polarization weather radar. part i: description of the polarimetric radar variables. *J. Operational Meteorology* 1, 226–242. doi:10.15191/nwajom.2013.0119

List, R., and de Quervain, M. (1953). Zur struktur von hagelkörnern. *Z. für Angew. Math. Phys. ZAMP* 4, 492–496. doi:10.1007/bf02067905

Ludlam, F. (1958). The hail problem. *Nubila* 1, 12.

Macklin, W., Carras, J., and Rye, P. (1976). The interpretation of the crystalline and air bubble structures of hailstones. *Q. J. R. Meteorological Soc.* 102, 25–44. doi:10.1256/smsqj.43102

Michaud, A. B., Dore, J. E., Leslie, D., Lyons, W. B., Sands, D. C., and Priscu, J. C. (2014). Biological ice nucleation initiates hailstone formation. *J. Geophys. Res. Atmos.* 119, 12–186. doi:10.1002/2014jd022004

Pack, J. D., Xu, M., Wang, G., Baskaran, L., Min, J., and De Man, B. (2022). Cardiac CT blooming artifacts: clinical significance, root causes and potential solutions. *Vis. Comput. Industry, Biomed. Art* 5, 29–13. doi:10.1186/s42492-022-00125-0

Peralta, J. P., Ibañez, J. C., and Juaneda, A. (2019). Comparison of hounsfield units obtained from cone beam tomographies, analyzed by 3 different software (in Spanish), 1–36. doi:10.13140/RG.2.2.26584.03846

Rauber, R. M., Charlevoix, D. J., and Walsh, J. E. (2005). *Severe and hazardous weather: an introduction to high impact meteorology*. Dubuque, Iowa: Kendall/Hunt Pub. Co.

Rigo, T., and Farnell, C. (2023a). A comparative analysis between radar and human observations of the giant hail event of 30 August 2022 in Catalonia. *Atmosphere* 14, 1190. doi:10.3390/atmos14071190

Rigo, T., and Farnell, C. (2023b). A summary of hail events during the summer of 2022 in Catalonia: a comparison with the period of 2013–2021. *Remote Sens.* 15, 1012. doi:10.3390/rs15041012

Rigo, T., and Farnell, C. (2023c). The variability of hailfall in Catalonia and its climatic implications. *Climate* 11, 16. doi:10.3390/cli11010016

Rigo, T., Rodríguez, O., Bech, J., and Farnell, C. (2022). An observational analysis of two companion supercell storms over complex terrain. *Atmos. Res.* 272, 106149. doi:10.1016/j.atmosres.2022.106149

Shedd, L., Kumjian, M. R., Giammanco, I., Brown-Giammanco, T., and Maiden, B. R. (2021). Hailstone shapes. *J. Atmos. Sci.* 78, 639–652. doi:10.1175/jas-d-20-0250.1

Sneed, E. D., and Folk, R. L. (1958). Pebbles in the lower Colorado River, Texas a study in particle morphogenesis. *J. Geol.* 66, 114–150. doi:10.1086/626490

Soderholm, J. S., and Kumjian, M. R. (2023). Automating the analysis of hailstone layers. *Atmos. Meas. Tech.* 16, 695–706. doi:10.5194/amt-16-695-2023

Whitcher, B., Schmid, V. J., and Thornton, A. (2011). Working with the DICOM and NIfTI data standards in R. *J. Stat. Softw.* 44, 1–28. doi:10.18637/jss.v044.i06